Analyst

Accepted Manuscript

This article can be cited before page numbers have been issued, to do this please use: R. Chen, B. Liu, H. Ni, N. Chang, C. Luan, Q. Ge, J. Dong and X. Zhao, *Analyst*, 2019, DOI: 10.1039/C9AN00733D.

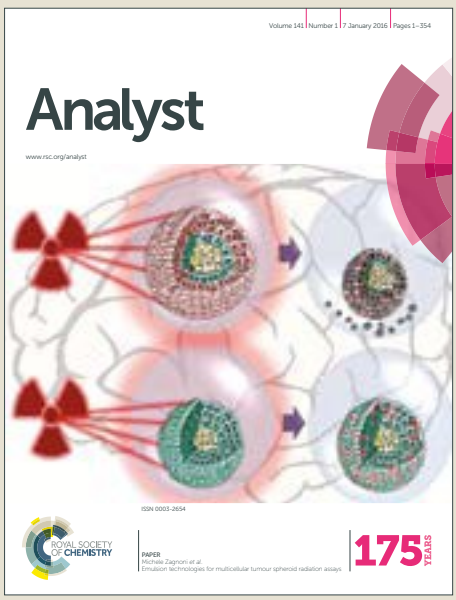

ROYAL SOCIETY OF CHEMISTRY

rsc.li/analyst

View Article Online
DOI: 10.1039/C9AN00733D

ARTICLE

Vertical Flow Assays Based on Core-Shell SERS Nanotags for Multiplex Prostate Cancer Biomarkers Detection†

Received 00th January 20xx,
Accepted 00th January 20xx

DOI: 10.1039/x0xx00000x

Ruipeng Chen,[‡abc] Bing Liu,[‡abc] Haibin Ni,[ab] Ning Chang,[ab] Chengxin Luan,[d] Qinyu Ge,[ab] Jian Dong,[ab] and Xiangwei Zhao*[abc]

Rapid, simultaneous, and sensitive quantification of multiplex prostate biomarkers plays an important role in early diagnosis, especially for obese men and patients. Herein, a surface-enhanced Raman scattering (SERS)-based vertical flow assay (VFA) is presented for simultaneous detection of multiplex prostate cancer biomarkers, such as prostate-specific antigen (PSA), carcinoembryonic antigen (CEA), and alpha-fetoprotein (AFP) on a single test spot. In practice, Raman dyes (RDs) encoded core-shell SERS nanotags instead of conventional gold colloids used in the colorimetric assay are employed in the sensing membrane of SERS based VFA for multiplex proteins detection. Because of the enhanced Raman signal of the core-shell nanostructure and the high surface area to volume ratio (SVR) of the porous sensing membrane, this proposed biosensor shows wide linear dynamic range (LDR) with detection limits of 0.37, 0.43, and 0.26 pg mL^{-1} for PSA, CEA, and AFP, respectively, suggesting that this approach can be a good candidate in point of care testing (POCT) for rapid and sensitive biomarkers detection and has a prosperous potential in multiplex analysis and cancer diagnosis.

Keywords: vertical flow assay, core-shell SERS nanotags, multiplex detection, prostate cancer biomarkers, POCT

Introduction

Multiple identification and quantification of protein biomarkers are increasingly important for accurate diagnosis, monitoring, and prognosis of complex diseases such as cancer.[1,2] Prostate cancers are currently the most prevalent form of cancer in men and the second leading cause of male cancer death. Prostate-specific antigen (PSA), a serine protease, is detectable in serum has proved to be an extremely valuable marker for early detection of prostate cancer.[3,4] However, a high PSA level (the normal cutoff value in serum is < 4 ng mL^{-1}) is not specific for diagnosis of prostate cancer because PSA can be elevated by other conditions.[5] To improve the screening accuracy prior to a prostate biopsy, more analytes are needed to be detected in a single test to increase the information throughput of health monitoring. For example, multiplex prostate related biomarkers, such as prostate-specific antigen (PSA), carcinoembryonic antigen (CEA), and alpha-fetoprotein (AFP) are needed to be detected for the quick and accurate diagnosis of prostate cancer.

Nowadays, lots of diagnostic techniques have been developed for biomarkers detection, such as polymerase chain reaction (PCR) assays,[6] enzyme-linked immunosorbent assay (ELISA),[7] chemiluminescent,[8] and electrochemical assays (ECA).[9] However, due to the complex operation process and limited availability of laboratory infrastructure as well as financial support, they are not widely used in ordinary families. Compared with standard laboratory testing, vertical flow assay (VFA), as an immunofiltration assay, is most widely employed in point of care testing (POCT) field because of the evident advantages, such as simple operation, faster analysis, and the absence of false-negative including hook effect.[10] Moreover, conventional VFA is paper-based gold-conjugated immunoassay and gold colloids are the most widely used in POCT technology owing to its simple preparation, stability, and robustness in various applications.[11-14] Nevertheless, conventional VFA usually uses eyes to analyze gold nanoparticles (AuNPs) conjugated antibody targets with the characteristic reddish color, which may suffer from poor precision and limited sensitivity.

In order to improve the precision and sensitivity of VFA, various detection labels, such as magnetic particles,[15,16] fluorescence microspheres[17,18], and carbon nanoparticles[19] combined with optical reader have attracted a lot of attention. However, fluorescence is amenable to quenching and bleaching and usually affected by the background of the substrate. Carbon nanoparticles and magnetic labels still suffer from poor sensitivity and low precision for trace analysis. Recently, surface enhanced Raman scattering (SERS) has been investigated as an

[a] State Key Laboratory of Bioelectronics, School of Biological Science and Medical Engineering, Southeast University, Nanjing 210096, China. E-mail: xwzhao@seu.edu.cn
[b] National Demonstration Center for Experimental Biomedical Engineering Education, Southeast University, Nanjing 210096, China
[c] Key Laboratory of Environmental Medicine Engineering of Ministry of Education, Southeast University, Nanjing 210096, China
[d] Department of Hematology and Oncology (Key Department of Jiangsu Medicine), Zhongda Hospital, School of Medicine Southeast University, Nanjing 210009, China
‡The two authors contributed equally to this work.
†Electronic Supplementary Information (ESI) available. See DOI: 10.1039/x0xx00000x

View Article Online
DOI: 10.1039/C9AN00375D

alternative analytical chemistry techniques for chemical and biomolecule analysis, due to its advantages such as photostability, non-destructive, and ultra-sensitivity of single molecule level.[20-24] Therefore, combining the advantage of SERS and VFA, SERS based VFA will have a prosperous potential for biomarkers analysis and disease diagnosis. To our knowledge, SERS-based VFA had been previously reported by two research groups, one report measured Flucytosine in serum, with a limit detection of 12.1 mg mL^{-1}, covering the clinically relevant therapeutic range.[25]Another report demonstrated the detection of Hepatitis C (HCV) with the detection limits of 1/1024 diluted antibody.[26] However, both of them detect a single biomarker with the aid of AuNPs or AgNPs to enhance single Raman peak which is not useful for obtaining high throughput bioinformatics data. Additionally, AuNPs/AgNPs-based enhanced Raman signal has limited effect on signal-to-noise ratio. As the width of the Raman peak is about 10-100 time narrower than that of fluorescence emission peak.[27] This is beneficial for reducing the interference between different Raman dyes (RDs), making it an excellent encoding element in multiplex SERS based bioassays.[28,29] In our group, RDs encoded core-shell (Au@Ag) nanostructure-based SERS nanotags have been synthesized and applied to multiplex bioassays. Compared with bare metal NPs, the signal of the embedded Raman dyes (RDs) could be greatly amplified, because of the high-efficiency plasmon-enhanced Raman scattering of the core-shell gap, which allows for ultrasensitive quantitative biological assays.[30,31]

In this study, we proposed a multiplex VFA based on RDs encoded core-shell SERS nanotags as labels for quantitative and rapid detection of three prostate biomarkers, PSA, CEA, and AFP on a single test spot (Fig. 1). As shown in Fig. 1a, gold core and silver shell bimetallic nanoparticles with three kinds of RDs encapsulated in the interior-gap to form Au^{NBA}@Ag, $Au^{4\text{-}MB}$@Ag, and $Au^{4\text{-}NBT}$@Ag core-shell SERS nanotags and subsequently were conjugated with detection antibodies against PSA, CEA, and AFP, respectively. The structure of SERS-based VFA biosensor was consisted of two layers of material (Fig. 1b). The upper layer material was nitrocellulose (NC) membrane, which was used as sensing membrane, and the bottom layer was composed of absorption pads. Finally, the two layered structures were encapsulated in a cartridge. Importantly, one single test spot composed of capture antibodies against PSA, CEA, and AFP with the molar ratio of 1:1:1 were immobilized on the sensing membrane for multiplex analysis (Fig. 1b). The procedures of the SERS-based VFA are described as follows. First, analytes containing different concentrations of PSA, CEA, and AFP and three kinds of detection antibodies conjugated SERS nanotags were placed in a tube for immunoreaction. Then, the complex flowed through the sensing membrane. Afterward, the sensing membrane was washed three times with washing buffer. Finally, the mixed Raman spectrum was measured and analyzed for multiplex quantitative immunoassay detection. It's worth noting that the assay procedure could be completed within about 7 min, which greatly reduced the cost of time. Furthermore, the first immunoreaction was carried out in the tube, resulting in the enhancement of the reaction uniformity because of the homogeneous system, which boosted the robustness of the VFA compared with the common two-step titration reaction.

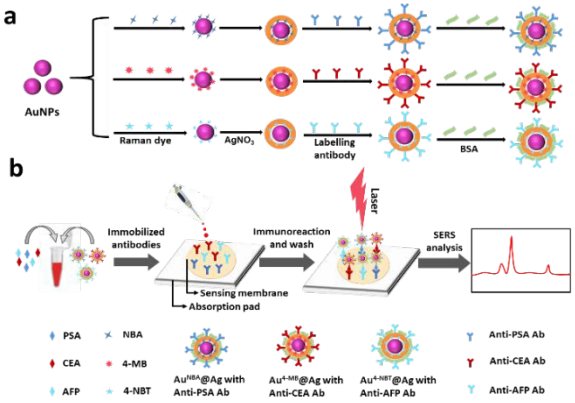

Fig. 1 Experimental schematic illustration of (a) the synthesis of multiplex core-shell SERS nanotags and (b) multiple prostate cancer biomarkers detection by core-shell SERS nanotags combined with VFA.

Experiment

Materials and chemicals

Silver nitrate ($AgNO_3$), tetrachloroaurate (III) trihydrate ($HAuCl_4 \cdot 3H_2O$), trisodium citrate ($Na_3C_6H_5O_7$), and bovine serum albumin (BSA) were purchased from Sigma (St. Louis, MO, USA). 4-Mercaptobenzonitrile (4-MB), 4-Nitrobenzenethiol (4-NBT), Nile blue A (NBA), and ascorbic acid were received from Alfa Aesar. Phosphate buffered saline-Tween-20 (PBST, 0.05 % Tween-20 in PBS), K_2CO_3 (0.1 M), HCL (0.1 M) and phosphate buffer saline (PBS, 0.01 M, pH 7.4) were prepared in-house. All glassware were first soaked in freshly prepared aqua regia solution (HCl/HNO_3, v/v, 3:1) overnight and then rinsed thoroughly with deionized water before use.

Human alpha-fetoprotein (AFP), carcinoembryonic antigen (CEA), and Prostate-specific antigen (PSA), as well as a pair of anti-AFP monoclonal antibodies, anti-CEA monoclonal antibodies, and anti-PSA monoclonal antibodies produced in goats, were purchased from Beijing Key-bio Biotech Co., Ltd. (China). Nitrocellulose membranes were acquired from Kenker (USA). Absorption pad was purchased from Beijing GE Healthcare Life Sciences, Co., Ltd (China). All aqueous solutions were prepared using deionized water (18 MΩ) obtained from a Milli-Q system (Millipore S.A., Bedford, USA). Clinical serum samples were collected from Zhongda Hospital Affiliated to Southeast University and approved by its Institutional Ethics Committee.

Preparation of the sensing membrane

The commercially available NC membranes were small circle piece pads with a diameter about 13 mm, and they were placed in an ultrasonic instrument containing 95 % pure ethanol for 30 s for the transparency process and then tiled on the glass wafer. After that, they were washed with PBS buffer for several times. Subsequently, we immobilized PSA, CEA, and AFP capture

antibodies (1.0 μg/mL, v/v/v, 1:1:1) on the NC membranes with a pipette to form a modified test zone for multiplex detection. After which, the NC membranes were put into the shaker and incubated at 37 °C for 1 h. Finally, 2 % (wt/wt) BSA solution was employed to block the nonspecific adsorption sites. After washing three times with PBS buffer, the prepared sensing membranes were stored in 4 °C for further use.

Synthesis of core-shell SERS nanotags

The core-shell SERS nanotags were prepared by using a seed-growth colloid technique from those previously reported.[32,33] Gold colloids were first synthesized based on the method of citrate thermal reduction and these gold nanoparticles were used as seeds for SERS nanotags preparation.[21,34] Afterward, three kinds of RDs, NBA (1.0 μM, 500 μL), 4-MB (5.0 μM, 500 μL), and 4-NBT (5.0 μM, 500 μL) were added dropwise to AuNPs (5 mL) and reacted for 1 h under magnetic stirring. Then, the reporters bound AuNPs were centrifuged at 8000 rpm for 15 min to discard unbound Raman reporter molecules, and the sediment was resuspended in 5 mL ultrapure water. After that, 500 μL of 0.1 M ascorbic acid was added to the above functionalized Au@^{NBA}, Au@$^{4\text{-}MB}$, and Au@$^{4\text{-}NBT}$ colloid solution in a conical beaker under magnetic stirring. Subsequently, 500 μL of 1 mM $AgNO_3$ was added dropwise to the above conjugated colloids by micropipette with vigorously stirring for 40 min, because of the $AgNO_3$ was reduced by ascorbic acid, the color of the conjugated solution changed from purple-pink to orange-yellow indicated that the resultant Ag shells continuously grew on the surface of conjugated gold seeds. After being centrifuged at 10000 rpm for 10 min and discarding of the supernatant, the core-shell SERS nanotags of Au^{NBA}@Ag, Au$^{4\text{-}MB}$@Ag and Au$^{4\text{-}NBT}$@Ag were obtained and resuspended in the same volume of PBS for further use.

Preparation of bio-functioned core-shell SERS nanotags

For multiplex detection of PSA, CEA, and AFP antigens, three sets of distinct core-shell SERS nanotags (Au^{NBA}@Ag, Au$^{4\text{-}MB}$@Ag, and Au$^{4\text{-}NBT}$@Ag) were used for specific recognition of each target antigen. First, the pH value of the nanoparticles solution was adjusted to 8.5 with 0.1 M K_2CO_3 and HCL, then 2 mL of Au^{NBA}@Ag, Au$^{4\text{-}MB}$@Ag, and Au$^{4\text{-}NBT}$@Ag solutions were mixed with PSA-Ab, AFP-Ab, and CEA-Ab (10 μg/mL, 50 μL), respectively, and incubated for 1 h at 37 °C, then 2 % BSA was added to block the bio-functioned SERS nanotags overnight. Following the overnight incubation, the bio-conjugated NPs were centrifuged to remove unbound antibodies and minimize non-specific interactions. Afterward, the bio-functioned NPs were resuspended in the same volume of PBS and stored in 4 °C for further use.

Instruments

The characterization of AuNPs and SERS nanotags were implemented by scanning electron microscopy (SEM; Zeiss, Ultra Plus) and transmission electron microscopy (TEM; JEOL, JEM-2100), respectively. The microstructure of the NC membrane was recorded by SEM, and the SEM results showed that the pore size distribution was in the range of 0.45 ± 0.05 μm. The absorption spectrum of AuNPs was measured using Hitachi 5000 UV/Vis/NIR spectrophotometer.

The Raman spectra and SERS mapping images for the test zone of the sensing membranes were carried out using an InVia Renishaw Raman microscope system (Renishaw). Here, a He-Ne laser Raman excitation source with a power of 7.4 mW at an operating wavelength of 785 nm was utilized. The Raman spectrum measurement system was calibrated using silicon wafer with Raman shift at 520 cm^{-1}, as well as a charge-coupled device (CCD) camera coupled to a spectrograph to provide a high-resolution Raman spectrum of 1 cm^{-1}. In order to remove the Rayleigh line, a holographic notch filter was placed in the collection path. Baseline correction and removal of fluorescence band of each Raman spectrum was performed using Renishaw Wire 4.2 software. The characteristic Raman shift of RDs, NBA, 4-MB, and 4-NTB are at 593, 1074, and 1343 cm^{-1} respectively. Raman mapping images were received using a 20× objective lens with the numerical aperture of 0.40.

Results and discussion

SERS-based VFA analysis

As a proof of concept, we used the as-proposed biosensor for the simultaneous detection of PSA, AFP, and CEA on a single test spot. Briefly, 30 μL PSA, CEA, and AFP antigens of different concentrations (1:1:1, v/v/v, from 0 fg mL^{-1} to 100 μg mL^{-1}) were first mixed with the prepared bio-conjugated NPs for about 2 min at room temperature. Then, 10 μL of the mixture was dropped on the antibodies modified spot of the sensing membrane, and kept it for 3 min, by increasing the reaction time, to improve the immunoreaction efficiency. Afterward, the test spot was washed three times (20 μL with 40 s interval for each washing) with PBST to remove the non-reacted SERS nanotags. Finally, the sensing membrane was excited with Raman microscope, and the mixed Raman spectrum was measured and deconvoluted with a multivariate method for multiplex quantitative immunoassay analysis.

Characterization of SERS nanotags

The core-shell structure of the SERS nanotags is schematically illustrated in Fig. 1a and the TEM image of the core-shell NPs are shown in Fig. 2a, it can be seen that the as-prepared core-shell SERS nanatags are well-dispersive and their average size is about 65 nm in diameter, as shown in Fig. 2b. In our method of multiplex assays, the SERS nanotags act as labels for quantitative analysis. Therefore, the Raman signal of SERS nanotags should be taken into attentive consideration for high intensity and reproducible detection. Since Raman signal of SERS nanotags is greatly depended on the electromagnetic enhancement originated from the localized surface plasmon resonance (LSPR) of core-shell (Au@Ag) NPs which is wavelength-modulated by incident light.[35-38] Hence, the excitation source was selected first according to the E field enhancement and distribution of the core-shell NPs obtained by FDTD simulation (FDTD Solutions, Lumerical Inc.). Moreover, the construction of the FDTD simluation model is based on the TEM image of core-shell nanostructure, as shown in Fig. S1a (Supporting Information). From the simulation results (Fig. S1b-

View Article Online
DOI: 10.1039/C9AN00755D

d, Supporting Information), it can be seen that the enhanced E field distribution (named as "hotspots") of the core-shell nanostructure is mainly confined in the gap, and with high intensity under the excitation of 785 nm laser. Whereas, under the excitation of 532 and 633 nm lasers, the hotspots are mainly distributed on the surface of the core-shell NP, which has no signification for the signal enhancement of the RDs. Thus, we used the 785 nm laser throughout the experiment. Under the optimal conditions, RDs were embedded in the interior gap between gold core and silver shell, and the resultant SERS nanotags were used as labels. Then, UV-vis absorption spectra were used to confirm the conjugation of antibody on the surface of Au@^{NBA}Ag NPs and the monodispersity of the conjugated NPs.[39] From Fig. 2c, it could be seen that the characteristic absorption peak of AuNPs with a diameter of about 60 nm is 530 nm, and it shifts to 533 nm after RDs (NBA) absorption, and then blue-shift to 510 nm, providing the strong evidence for the growth of Ag shell. Subsequently, the absorption peak red-shift from 510 to 538 nm following the incubation of antibodies, indicating the successful immobilization of antibodies. All these surface plasmon band shifts in accordance with the traditional Mie scattering theory and the support of dielectric data.[40,41] In addition, it can also be seen that the full width at half maximum (FWHWs) of the absorption peaks for AuNPs, Au^{NBA} NPs, and Au^{NBA}@Ag NPs solutions were not significantly changed, which provides the evidence for the uniform particle size and monodispersity of these nanotags. Whereas, the absorption peak of Au^{NBA}@Ag@Antibody is lower and the FWHW is wider than the above NPs which stems from the attachment of antibodies on the surface of core-shell nanotags, causing the change of particle size, shape and monodispersity.[39] In order to check the SERS signal of the functionalized SERS nanotags, we then investigated the intensity of the Raman signal at successive steps in the synthesis of antibody conjugated SERS nanotags, as shown in Fig. 2d. It can be seen the Raman intensity is significantly enhanced of Au core Ag shell bimetallic NPs (Au@Ag) compared with bare RDs (NBA) or Au^{NBA} NPs. In addition, the SERS signals of antibodies conjugated SERS nanotags is also very fine and the SERS background is inconsequential, which is valuable for the achievement of high signal-to-noise ratio and in in favor of quantitative bioassay analysis.[36] These characteristic results confirm the SERS nanotags are sensitive and stable for quantification in immunoassays detection.

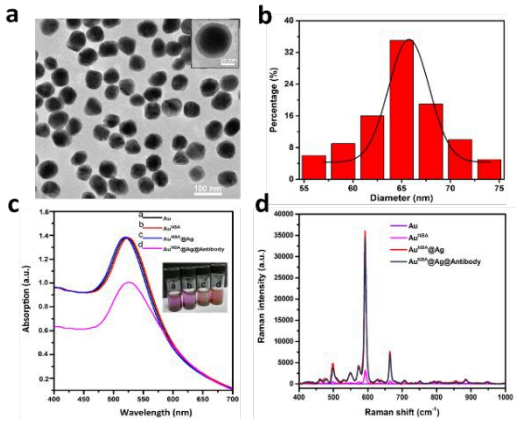

Fig. 2 (a) TEM image and (b) statistical size distribution of core-shell SERS nanotags, (c) UV-vis absorption spectra and (d) Raman spectra of SERS nanotags at different synthesis steps. Inset: Digital picture showing the color change of NPs solutions

Analysis of SERS spectra

In order to simultaneously detect multiplex prostate biomarkers in a single test spot of SERS-based VFA by Raman spectra, three kinds of RDs decorated gold-silver core-shell SERS nanotags Au^{NBA}@Ag, $Au^{4\text{-}MB}$@Ag, and $Au^{4\text{-}NBT}$@Ag were selected as encoded labels with accordingly three easily distinguished characteristic Raman shifts at 593, 1074, and 1343 cm^{-1}. Specifically, it is worth noticing that the sensing nitrocellulose (NC) membrane also inherently has nitro group, in order to confirm if there is some extent interference by NC on $Au^{4\text{-}NBT}$@Ag. We perform SRES test for $Au^{4\text{-}NBT}$@Ag with NC, as shown in Fig. S2 (Supporting Information), the intensity of the characteristic SERS spectrum of NC is much weaker compared with $Au^{4\text{-}NBT}$@Ag, in addition, there is no obvious spectra overlap between NC and $Au^{4\text{-}NBT}$@Ag. Hence, $Au^{4\text{-}NBT}$@Ag is suitable with the other two encoded SERS nanotags for multiplex prostate biomarkers detection. Critically, the intensity of single SERS nanotag should be consistent for distinguishing analystes and determining their concentrations on test spot, since it is pivotal to improve the detection accuracy. Therefore, to confirm the coding capacity as well as the Raman intensities of the SERS nanotags, Raman spectra collected from PSA antibody conjugated Au^{NBA}@Ag, CEA antibody conjugated $Au^{4\text{-}MB}$@Ag, AFP antibody conjugated $Au^{4\text{-}NBT}$@Ag, and equimolar mixture (v/v/v, 1:1:1) of these functionalized NPs were shown in Fig. 3a. Although the Raman shifts at 1074 cm^{-1} of 4-MB and 1088 cm^{-1} of 4-NBT were very close, as well as the Raman shifts at 1343 cm^{-1} of 4-MB and 1334 cm^{-1} of 4-NBT, there is no overlap between them (Fig. S3, Supporting Information). Notably, the measured mixed Raman spectrum could be distinguished three main individual components with a multivariate deconvolution by weighted least-squares residuals method shown in Fig. 3b.[42] Here, the marked characteristic Raman peaks of NBA (593 cm^{-1}), 4-MB (1074 cm^{-1}), and 4-NBT (1343 cm-1) were proved to have no overlaps among each other. Moreover, the percentage of deconvoluted Raman intensity of equimolar mixture spectrum at 593, 1074, and 1343 cm^{-1} were calculated to be 82.2, 83.2, and 81.6 %, respectively (Fig. S4, Supporting Information). It can be seen that the intensities are almost the same for the three SERS nanotags and are satisfactory for the multiplex and quantitative detection in single test spot of SERS-based VFA system.

View Article Online
DOI: 10.1039/C9AN00733D

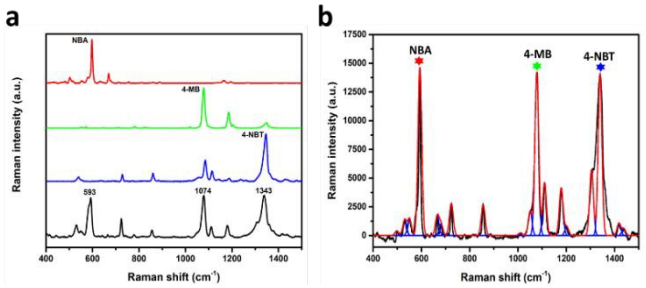

Fig. 3 (a) Three kinds of Raman spectra of functionalized Au^{NBA}@Ag (red line), $Au^{4\text{-}MB}$@Ag (green line), $Au^{4\text{-}NBT}$@Ag (blue line), and their equal molar (v/v/v, 1:1:1) mixture (black line). The marked Raman peaks at 593, 1074, and 1343 cm^{-1} are unique to NBA, 4-MB, and 4-NBT, respectively. (b) Raman spectrum of the equimolar mixture of functionalized Au^{NBA}@Ag, $Au^{4\text{-}MB}$@Ag, and $Au^{4\text{-}NBT}$@Ag SERS nanotags was deconvoluted into three distinctive peaks (black line). Red line represents the Gauss Fit of the overall measured spectrum. Blue line stands for Gauss Fit of the characteristic Raman shifts of the measured spectrum.

Selection of mapping area of test point for quantification

Due to the feature of the porous NC membranes, the distribution of hot spots in test zone is not homogeneous, which caused serious fluctuation of Raman signal, and the accuracy of quantitative measurement will be extremely affected.[43] Besides, in most cases, it is difficult to achieve a highly homogeneous spatial distribution of hot spots on the substrate even though the surface morphology and detection conditions are carefully controlled. In order to solve this problem for quantification analysis in SERS-based VFA, it is more important to select the sampling region reasonably. According to the previous report, sampling errors can be curtailed by increasing the sample region.[44] In our SERS-based VFA, an alternative approach to increase sampling size is to increase the spatial mapping test zone and obtain the averaged SERS signal in a larger area, so as to achieve a reproducible intensity value. Here, three different mapping models were depicted in Fig. 4a-c and their performance with different concentrations PSA were analyzed in Fig. 4d. For each experiment, 10 μL of the analyte solution of different concentration was dropped onto the sensing membrane (The average diameter of the test zone was ~3 mm) and then washed. The whole test zone (3200 × 3200 μm) was selected for mapping area in Fig. 4a with the mapping step of 100 × 100 μm. In Fig. 4b and c, mapping area of 1000 × 1000 μm was selected from the central part of the test zone with a mapping step of 100 × 100 μm and 20 × 20 μm, respectively. The laser power was fixed to be 7.4 mW. The total acquisition time were 3072, 363, and 7803 s for Fig. 4a-c, respectively. After sample detection, the calibration curves of average Raman intensities using different sample concentration with three different mapping methods were plotted (Fig. 4d). The Raman intensity and R^2 value were all decreased with the whole mapping test zone (Fig. 4a). The Raman intensity and R^2 obtained from (Fig. 4c) were the highest, however, the time of Raman mapping was 7803 s (about 130 min), which is time-consuming for POCT detection. Taking consideration of time as well as Raman intensity and R^2, mapping model of Fig. 4b was chosen to realize quick quantification of our SERS-based VFA with a Raman mapping time of 363 s (about 6 min). With the increasing need for portable Raman instruments in the fast developing POCT market, our experiment results will provide some useful guidance to it.

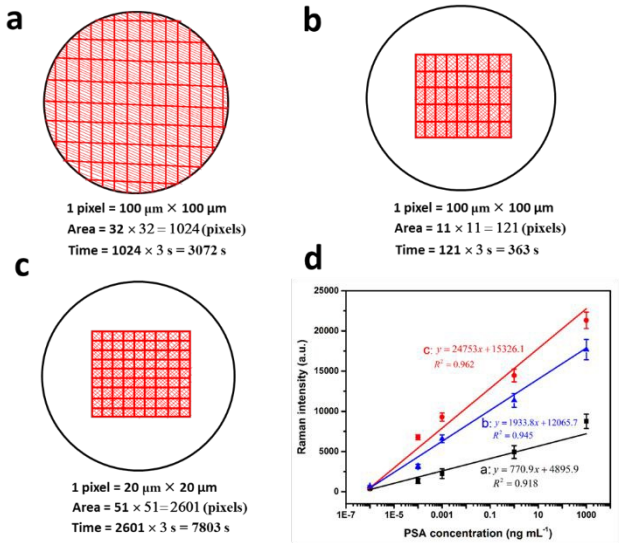

Fig. 4 (a, b and c) Schematic illustration of mapping with different models. (d) Corresponding calibration curves of average Raman intensities at Raman shift 593 cm^{-1} using PSA of different concentration with different mapping methods. Error bar is calculated from three Raman mapping repeats

Evaluation of the SERS based VFA biosensor

To assess the quantitative performance of the SERS based VFA biosensor by core-shell SERS nanotags, PSA as a detection biomarker was used for the validation of the platform in a sandwich immunoassay. First, PSA at concentrations of 100 μg mL^{-1} decreased to 100 fg mL^{-1} were mixed with Au@^{NBA}Ag labeled antibodies, and then dropwise add on the sensing membrane with a micropipette to enable forming the sandwich complex. After washing three times with PBST, SERS measurements were performed by point-to-point mapping on each sample (Fig. 5a) and the sampling methods have been illustrated in Fig. 4. The averaged SERS spectra with Raman shift at 593 cm^{-1} for each sample with different concentrations were shown in Fig. 5b. The relationship between the intensities of Raman shift at 593 cm^{-1} was plotted against the logarithm of PSA concentrations, as shown in Fig. 5c. It can be seen that with the increasing concentrations of PSA, the color of the sensing membrane at center position becomes brighter, and the Raman intensity is getting higher, exhibiting a wide linear dynamic range (LDR) of 0.001-1000 ng mL^{-1} (R^2 = 0.994), spanning 6 orders of magnitude. In addition, the limit of detection (LOD), calculated from the analyte concentration that produces a signal 3-fold higher than the standard deviation of blank measurements, was 0.18 pg mL^{-1}, which was also much lower than those previously reported.[45-47] These results can be attributed to several reasons, the first one is that the high surface area to volume ratio (SVR) of the sensing membrane that is favorable for combining more analytes. The second one is that the nanostructured core-shell SERS nanotags have stronger electromagnetic field enhancement which amplifies SERS signals greatly. The third one is that we employ three times washing of non-reacted SERS

View Article Online
DOI: 10.1039/C9AN00733D

nanotags on the sensing membrane with PBST solution in the assay practice (Fig. S5, Supporting Information). It can be seen that after three-round washing procedure the Raman intensity of sensing substrate decreased extremely, indicating most of the non-reacted SERS nanotags were removed, which improves the signal to noise ratio (SNR) of the biosensor. All the superior performances suggest that the SERS based VFA can achieve ultrasensitive detection of protein biomarkers with wider LDR, higher sensitivity and include the clinically relevant diagnostic range as well.

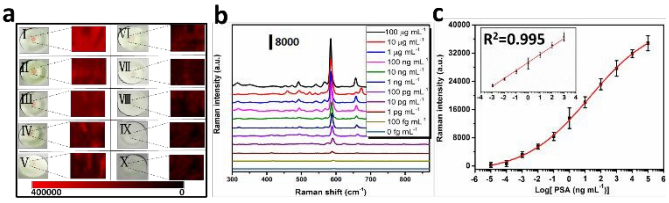

Fig. 5 Quantitative detection of PSA with SERS imaging technique. (a) Raman mapping of different concentrations of PSA (from 100 μg mL^{-1} decreased to 100 fg mL^{-1}, Ⅰ-Ⅹ). (b) Averaged Raman spectra for different concentrations of PSA (c) Reference plot of average Raman intensities at Raman shift 593 cm^{-1} vs logarithm of PSA concentrations. Error bar is calculated from three Raman mapping repeats. Inset is the linear part of the reference plot.

Multiplex biomarkers analysis on one point

Generally, cross-reaction is a common phenomenon in multiplex immunoassays and usually affects the detection results. Hence, we firstly perform the cross-reaction on the single test spot to evaluate the selectivity of the SERS based VFA (Fig. S6a-c, Supporting Information). After repeating these overall processes with three times, a statistical measurement of reproducibility was obtained as shown in Fig. S6d (Supporting Information), the variation coefficients (CV) of Raman signal for PSA, CEA and AFP were 12.3, 13.2, and 12.6 %, respectively. These results demonstrate a well functional SERS-based VFA that provides the recognition of SERS signatures with the correct analyte. For quantitative multiplex detection, we firstly immobilized the equimolar mixture of PSA, CEA, and AFP capture antibodies on the sensing membrane. Then, the multiplex biomarkers of PSA, CEA, and AFP (v/v/v, 1:1:1) with concentrations over a range of 100 μg mL^{-1}-0 fg mL^{-1} were performed, using aforementioned three kinds of functionalized SERS nanotags with characteristic Raman shift at 593, 1074, and 1343 cm^{-1} for PSA, CEA, and AFP, respectively. Subsequently, Raman mapping was conducted to measure the Raman intensity of the SERS nanotags on the single test spot as described above. From the Raman mapping images as shown in Fig. S7 (Supporting Information), it can be seen that the three kinds of immunocomplexes are evenly and randomly distributed on the test spot, which is favorable for obtaining the Raman signal of the three analytes in the test spot, and is also valuable for the reproducibility and reliability of the biosensor. Finally, the averaged SERS spectra measured within the test zone for multiplex biomarkers of different concentrations were shown in Fig. 6a. It can be seen that the Raman shift intensity at 593, 1074, and 1343 cm^{-1} increased gradually with the incremental concentration of PSA, CEA, and AFP that was consistent with the SERS mapping results.

Then, multiplex quantitative analysis of PSA, CEA, and AFP were conducted, and calibration curves were shown in Fig. 6b-d. All the three calibration curves with responsive range cover more than 10 orders of magnitude, which is improved more than three or four orders of magnitude in comparison with the conventional ELISA and colorimetric methods.[48] The reason may be that, compared with the conventional colorimetric assay used colloidal gold, when we use our functionalized core-shell SERS nanotags, the enhanced factor of the electric field lies the gap between the core and shell where the RDs located is about 1 × 10^8, leading to the detection sensitivity closed to a single molecule level.[29] The dose-responsive curves of PSA shown in the inset of Fig. 6b indicates a good linear relationship between the Raman intensity at 593 cm^{-1} and PSA concentration, with LDR spanning 6 orders of magnitude and the R^2 value of 0.982. From the quantitative analysis results of CEA and AFP (Fig. 6c and d, inset), it can be seen that both LDRs spanning 5 orders of magnitude with the R^2 value of 0.949 and 0.962, respectively. In addition, the LODs for PSA, CEA, and AFP were calculated to be 0.37, 0.43, and 0.26 pg mL^{-1} respectively, which were lower than that previous reports (Table S1, Supporting Information).[49-54] As far as we know, this is the first time three prostate biomarkers are quantitatively detected on a single test spot in SERS-based VFA. All the encouraging multiplex detection results suggest that this SERS-based VFA biosensor holds great promise for applications in practical clinical diagnosis and quantitative analysis of proteins in many fields like biological system, precision medicine, and so on.

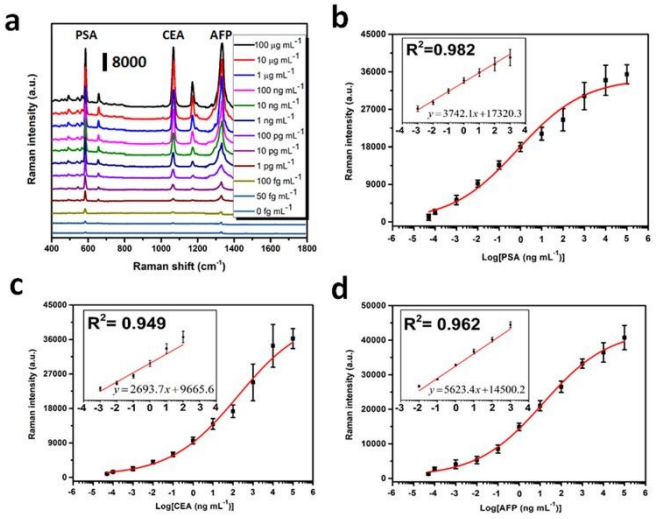

Fig. 6 (a) Averaged Raman spectra of test zone using Raman shift at 593, 1074, and 1343 cm^{-1} for the detection of three biomarkers (PSA, CEA, and AFP) at different concentrations over a range of 100 μg mL^{-1}-0 fg mL^{-1}; (b, c and d) Corresponding calibration curves of PSA, CEA, and AFP. Inset is the linear part of the reference plot. The error bars indicate the standard deviations calculated from three repeat measurements.

Clinical sample analysis

In order to verify the accuracy and practicability of SERS-based VFA in the clinical application, five different human serum samples, in which the concentration of PSA, CEA, and AFP range from 65.50 to 523.02 ng mL^{-1}, 28.87 to 313.02 ng mL^{-1}, and 156.13 to 659.9 ng mL^{-1} are shown in Table S2 (Supporting Information). First, the stability of the three kinds of the SERS nanotags (Au^{NBA}@Ag, $Au^{4\text{-}MB}$@Ag, and $Au^{4\text{-}NBT}$@Ag) in the human serum samples were investigated (Table S2, Supporting Information). The results illustrated that the coefficients of variation of the three kinds of SERS nanotags in serum samples were similar to that in water samples, which indicated that the stability of the core-shell SERS nanotags was good and could be used for the detection of human serum sample. Next, the samples were respectively measured with commercial electrochemiluminescent assay (ECLIA) kits in the hospital and the as-proposed method. The results showed in Fig. 7 demonstrate that the correlation coefficients between the two methods for multiplex detection of PSA, CEA, and AFP are 0.986, 0.988, and 0.992, respectively, and the recoveries of PSA, CEA, and AFP range from 96.2 to 108.5 %, 90.1 to 111.4 %, and 91.6 to 105.1 % (Table S3, Supporting Information), respectively, indicating the accuracy of the as-proposed multiplex assay is in good consistency with that of ECLIA. What's more, only 10 μL sample was used in our method which is much less than that used in ECLIA. In addition, SERS-based VFA holds the advantages of easy to use, convenient to transport and store, low cost, no tedious pretreatment, and no professional is needed in a clinical application. These results and advantages strongly illustrate that the multiplex signal test spot SERS-based VFA has great potential applications in clinical analysis.

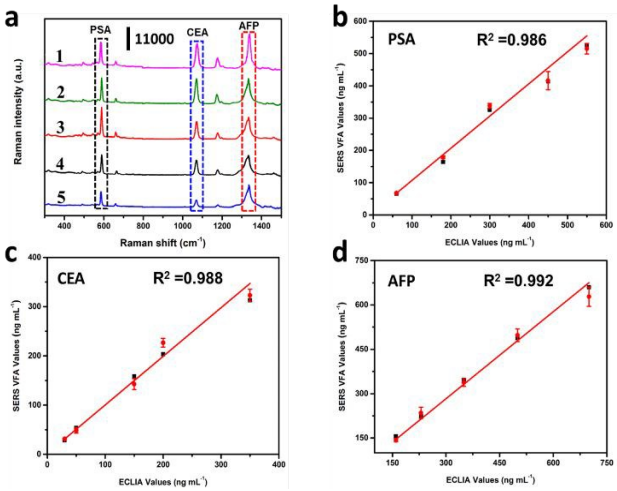

Fig. 7 Multiplex analysis of clinical serum samples on the single test spot SERS-based VFA. (a) Raman spectra of real human serum samples. Correlation of detection results acquired from SERS-based VFA (red circles) and reference ECLIA method (black squares) for (b) PSA, (c) CEA, and (d) AFP. Error bar is calculated from three repeats.

Conclusions

In summary, we proposed a POCT biosensor, which combined VFA with RDs encoded core-shell SERS nanotags for multiplex prostate biomarkers detection on a single test spot. SERS mapping technique was conceptually used in the as-proposed assay, so as to obtain a reproducible result with averaging hundreds of Raman spectra. The porous structure of the sensing membrane with high SVR could combine with more target biomarkers, which is favorable for extending the LDR to be from 1 pg mL^{-1} up to 10 μg mL^{-1} for PSA, and both from 10 pg mL^{-1} to 1 μg mL^{-1} for CEA and AFP. In addition, the core-shell nanostructure provides strong electromagnetic field enhancement, rendering the great amplification of Raman signal, which improves the detection sensitivity and the LODs of PSA, CEA, and AFP were calculated to be 0.37, 0.43, and 0.26 pg mL^{-1}, respectively. Moreover, the biosensor exhibited extremely low background, high stability, and reliability in real serum sample analysis. All these results indicated that our biosensor exhibited good analytical performance. In addition, the reagent consumption and cost are decreased, as well as the simplified operation procedure through recording multiplex spectra on a single test spot. We believe that the as-proposed biosensor can be easily extended to ultrasensitive detection of other biomarkers of general interest in the POCT field. Furthermore, SERS-based VFA will be combined with a portable Raman instrument with a large laser spot, which is more time-saving and convenient to operate, and also have great potential application in resources limited area.

Conflicts of interest

There are no conflicts of interest to declare.

Acknowledgements

This work was financially supported by the National Key Research and Development Program of China (No. 2018YFF0215200, 2017YFA0205700), National Natural Science Foundation of China (Grants 61850410528, 81827901 and 21327902), the Natural Science Foundation of Jiangsu Province (No. BK2014021828, BE2016002), China Postdoctoral Science Foundation funded project (2018M642132), the Fundamental Research Funds for the Central Universities, Six Talent Peaks Project of Jiangsu Province, the Collaboration Research Fund of Southeast University and Nanjing Medical University (Grant No. 2242017K3DN26), and Fundamental Research Project of Shenzhen Science & Technology innovation Committee (201803063001075).

Notes and references

1 G. H. Wu, R. H. Datar, K. M. Hansen, T. Thundat and R. J. Cote, A. Majumdar, *Nat. Biotechnol*, 2001, **19**, 856-860.
2 S. K. Vashist, P. B. Luppa, L. Y. Yeo, A. Ozcan and J. H. T. Luong, *Trends Biotechnol*, 2015, **33**, 692-705.
3 H. J. Chang, H. Kang, E. Ko, B. Jun, H. Lee, Y. Lee and D. H. Jeong, *ACS Sens.*, 2016, **1**, 645-649.
4 R. K. Gao, Z. Y. Cheng, X. K. Wang, L. D. Yu, Z. Y. Guo, G. Zhao and J. Choo, *Biosens. Bioelectron.*, 2018, **119**, 126-133.
5 K. Yang, Y. J. Hu, N. Dong, G. C. Zhu, T. F. Zhu and N. J.

Jiang, *Biosens. Bioelectron.*, 2017, **94**, 286-291.
6 B. Kavosi, A. Salimi, R. Hallaj and K. Amani, *Biosens. Bioelectron.*, 2014, **52**, 20-28.
7 A. H. Ahmed and H. M. E. Azzazy, *Biosens. Bioelectron.*, 2013, **49**, 478-484.
8 J. S. Lee, H. A. Joung, M. G. Kim and C. B. Park, *ACS Nano*, 2012, **6**, 2978-2983.
9 H. Zeng, D. A. Y. Agyapong, C. Li, R. Zhao, H. Yang, C. Wu, Y. Jiang and Y. Liu, *Sensor, Actuat. B-Chem.*, 2015, **221**, 22-27.
10 Y. K. Oh, H. Joung, S. Kim and M. Kim, *Lab Chip*, 2013, **13**, 768-772.
11 X. Xiao, T. P. Wang and Z. G. Tian, *J. Immunol. Methods*, 2003, **280**, 49-57.
12 T. Chinnasamy, L. I. Segerink, M. Nystrand, J. Gantelius and H. A. Svahn, *Clin. Chem.*, 2014, **60**, 1209-1216.
13 L. Rivas, P. Reuterswärd, R. Rasti, B. Herrmann, A. Mårtensson, T. Alfvén, J. Gantelius and H. Andersson-Svahn, *Talanta*, 2018, **183**, 192-200.
14 J. Park and J. K. Park, *Sensor. Actuat. B-Chem.*, 2017, **246**, 1049-1055.
15 D. Yang, J. Ma, Q. Zhang, N. Li, J. Yang, P. A. Raju, M. Peng, Y. Luo, W. Hui, C. Chen and Y. Cui, *Anal. Chem.*, 2013, **85**, 6688-6695.
16 J. Yan, Y. Y. Liu, Y. L. Wang, X. W. Xu, Y. Lu, Y. J. Pan, F. F. Guo and D. L. Shi, *Sensor. Actuat. B-Chem.*, 2014, **197**, 129-136.
17 B. Gao, H. Liu and Z. Z. Gu, *Anal. Chem.*, 2016, **88**, 5424-5429.
18 H. M. Joung, Z. S. Ballard, A. Ma, D. K. Tseng, H. Teshome, S. Burakowski, O. B. Garner, D. D. Carlo and A. Ozcan, *Lab Chip*, DOI: 10.1039/c9lc00011a
19 G. A. Posthuma-Trumpie, J. H. Wichers, M. Koets, L. B. J. M. Berendsen and A. V. Amerongen, *Anal. Bioanal. Chem.*, 2012, **402**, 593-600.
20 J. Liu, D. Y. Yin, S. S. Wang, H. Y. Chen and Z. Liu, *Angew. Chem. Int. Ed.*, 2016, **55**, 13215-13218.
21 B. Liu, X. W. Zhao, J. Wen, D. G. Fu and Z. Z. Gu, *Nanoscale*, 2016, **8**, 17465-17471.
22 J. Kneipp, H. Kneipp and K. Kneipp, *Chem. Soc. Rev.*, 2008, **37**, 1052-1060.
23 Z. Y. Cheng, N. Choi, R. Wang, S. Lee, K. C. Moon, S. Y. Yoon, L. X. Chen and J. Choo, *ACS Nano*, 2017, **11**, 4926-4933.
24 X. K. Wang, N. Choi, Z. Y. Cheng, J. Ko, L. X. Chen and J. Choo, Anal. Chem., 2017, **89**, 1163-1169.
25 A. G. Berger, S. M. Restaino and I. M. White, *Anal. Chim. Acta*, 2017, **949**, 59-66.
26 O. J. R. Clarke, B. L. Goodall, H. Hui, N. Vats and C. L. Brosseau, *Anal. Chem.*, 2017, **89**, 1405-1410.
27 J. M. Yu, J. Jeon, N. Choi, J. O. Lee, Y. Kim and J. Choo, *Sensor. Actuat. B-Chem.*, 2017, **251**, 302-309.
28 Y. Q. Wang, B. Yan and L. X. Chen, *Chem. Rev.*, 2013, **113**,1391-1428.
29 B. Liu, D. Zhang, H. B. Ni, D. L. Wang, L. Y. Jiang, D. G. Fu, X. F. Han, H. Y. Chen, Z. Z. Gu and X. W. Zhao, *ACS Appl. Mater. Interface*, 2018, **10**, 21-26.
30 B. Liu, H. B. Ni, D. Zhang, D. L. Wang, D. G. Fu, H. Y. Chen, Z. Z. Gu and X. W. Zhao, *ACS Sens*, 2017, **2**, 1035-1043.
31 X. L. Fu, Z. Y. Cheng, J. M. Yu, P. Choo, L. X. Chen and J. Choo, *Biosens. Bioelectron.*, 2016, **78**, 530-537.
32 Y. P. Huang, Y. Yang, Z. Chen, X. Li and M. Nogami, *J. Mater. Sci.*, 2008, **43**, 5390-5393.
33 Y. Xie, H. F. Chang, K. Zhao, J. G. Li, H. Yang, L. Y. Mei, S. M. Xu and A. P. Deng, *Anal. Methods*, 2015, **7**, 513-552.
34 G. Frens, *Nature-Physical Science*, 1973, **241**, 20-22.
35 S. Jia, C. Bian, J. Z. Sun, J. H. Tong and S. H. Xia, *Biosens. Bioelectron.*, 2018, **114**, 15-21.
36 T. X. Tan, C. G. Tian, Z. Y. Ren, J. Yang, Y. J. Chen, L. Sun, Z. T. Li, A. P. Wu, J. Yin and H. G. Fu, *Phys. Chem. Chem. Phys.*, 2013, **15**, 21034-21042.
37 J. N. Anker, W. P. Hall, O. Lyandres, N. C. Shah, J. Zhao and R. P. Van Duyne, *Nat. Mater.,* 2008, **7**, 442-453.
38 Q. Y. Xie, Y. H. Wu, Q. R. Xiong, H. Y. Xu, Y. H. Xiong, K. Liu, Y. Jin and W. H. Lai, *Biosens. Bioelectron.*, 2014, **54**, 262-265.
39 Y. Sun, L. Xu, F. D. Zhang, Z. G. Song, Y. W. Hu, Y. J. Ji, J. Y. Shen, B. Li, H. Z. Lu and H. F. Yang, *Biosens. Bioelectron.*, 2017, **89**, 906-912.
40 M. Moskovits, I. Srnová-Šloufová and B. Vlčková, *J. Chem. Phys.*, 2002, **116**, 10435-10446.
41 S. Bruzzone, G. P. Arrighini and C. Guidotti, *Mat. Sci. Eng. C*, 2003, **23**, 965-970.
42 N. Guarrotxena, Y. Ren and A. Mikhailovsky, *Langmuir*, 2011, **27**, 347-351.
43 D. Zhang, L. Huang, B. Liu, E. B. Su, H. Y. Chen, Z. Z. Gu and X. W. Zhao, *Sensor. Actuat. B-Chem.*, 2018, **277**, 502-509.
44 C. D. L. D. Albuquerque, R. G. Sobral-Filho, R. J. Poppi and A. G. Brolo, *Anal. Chem.*, 2018, **90**, 1248-1254.
45 D. D. Xu, Y. L. Deng, C. Y. Li, Y. Lin and H. W. Tang, *Biosens. Bioelectron.*, 2017, **87**, 881-887.
46 X. L. Fu, Y. Q. Wang, Y. M. Liu, H. T. Liu, L.W. Fu, J. H. Wen, J. W. Li, P. H. Wei and L. X. Chen, *Analyst*, 2019, **144**, 1582-1589.
47 N. Zhao, Y. Q. He, X. Mao, Y. H. Sun, X. B. Zhang, C. Z. Li, Y. H. Lin and G. D. Liu, *Electrochem. Commun.*, 2010, **12**, 471-474.
48 M. Lee, S. Lee, J. Lee, H. Lim, G. H. Seong, E. K. Lee, S. Chang, C. H. Oh and J. Choo, *Biosens. Bioelectron.*, 2011, **26**, 2135-2141.
49 Z. F. Wang, N. Liu, F. Feng and Z. F. Ma, *Biosens. Bioelectron.*, 2015, **70**, 98-105.
50 X. Chen, X. L. Jia, J. M. Han, J. Ma and Z. F. Ma, *Biosens. Bioelectron.*, 2013, **50**, 356-361.
51 J. N. Tian, L. J. Zhou, Y. C. Zhao, Y. Wang, Y. Peng and S. L. Zhao, *Talanta*, 2012, **92**, 72-77.
52 S. J. Xu, Y. Liu, T. H. Wang and J. H. Li, *Anal. Chem.*, 2011, **83**, 3817-3823.
53 B. Zhang, X. Zhang, H. H. Yan, S. J. Xu, D. H. Tang and W. L. Fu, *Biosens. Bioelectron.*, 2007, **23**, 19-25.
54 Q. Zhu, Y. Q. Chai, R. Yuan and Y. Zhuo, *Anal. Chim. Acta*, 2013, **800**, 22-28.

Journal Name ARTICLE

For TOC only

View Article Online
DOI: 10.1039/C9AN00733D

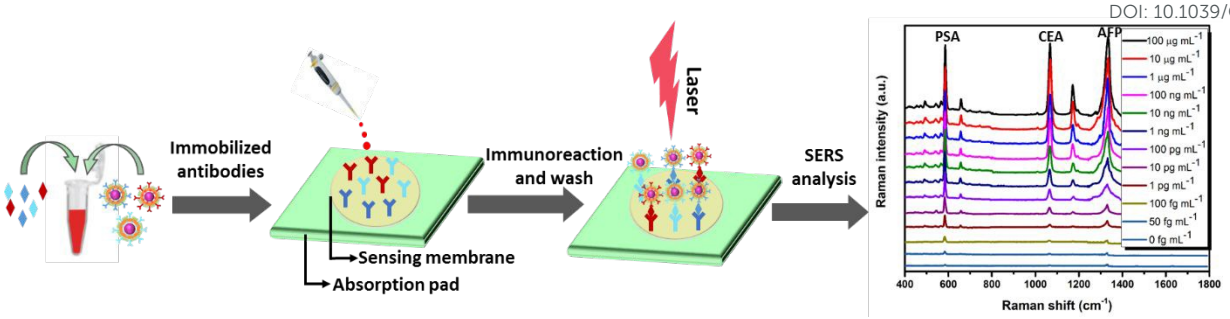

Highlight:

Core-shell SERS nanotags based VFA with single test spot for multiplex biomarkers detection at pg mL^{-1} level with wide LDR.